Quantum Electronics **38** (1) 64 – 68 (2008)

INTERFEROMETRY

PACS numbers: 42.40.Kw; 42.87.Bg
DOI: 10.1070/QE2008v038n01ABEH013496

Optical processing of holographic lateral shear interferograms recorded by displacing an object

A.M. Lyalikov

***Abstract*. A new approach is considered which is used in holographic lateral shear interferometry and allows the combination of the displacement of a phase object under study during the recording of holographic interferograms with the optical processing of displaced and optically conjugate holographic interferograms. Depending on the method of optical processing of such a pair of holographic interferograms, several aberration-free interference patterns are observed, which reflect with different sensitivities variations in the light wave phase caused by the phase object. Due to the lateral shear, which is equal to or exceeds the linear size of the object, the interference patterns of the object are identical to interference patterns obtained in a two-beam, reference-wave interferometer. The possibility of using this method to control optical inhomogeneities in active crystals in solid-state lasers is studied experimentally.**

Keywords: *holographic interferometry, phase object, lateral shear, compensation of aberrations, enhancement of the measurement sensitivity*.

1. Introduction

Shearing interferometers are stable to vibrations, simple to adjust, and their sensitivity compares well with two-beam, reference-wave interferometers. Among a variety of methods for producing a shear between two identical wave fronts, the lateral shear interferometry has received the widest acceptance [1, 2] and is now widely used in various fields of science and technology [3 – 8].

The main feature of lateral shear interferometry is the dependence of the behaviour of interference fringes on the relation between the shear value and the size of the object as well as on the shear value itself. If the object occupies only a part of the working field and its size is smaller than the shear, the interference fringes obtained in interferograms are the same as in the case of two-beam reference-wave interferometry [9]. This particular case of the lateral shear interferometry deserves a special attention because it combines the advantages of the two given methods. First of all, the interpretation of the interference pattern is simplified, which is complicated in the shearing interferometry. In the particular case considered above, the behaviour of interference fringes directly reflects a change in the phase of a probe wave caused by the object.

The measurement sensitivity in the lateral shear interferometry when the shear is larger than the object size can be increased by using the successive double lateral shear [10]. In this case, a moire pattern is observed, which reflects with a doubled sensitivity real-time changes in the phase of a probe light wave introduced by the object. The holographic variant of successive double lateral shear interferometry based on the optical processing of a pair of shifted holographic lateral shear interferograms provides the doubling of the measurement sensitivity or even improves it by four times [11]. However, these methods of increasing the measurement sensitivity involve residual aberrations related to the lateral shear of the probe beam [10] or holographic interferograms [11], which increases the requirements to the quality of optical elements of a lateral shear interferometer.

In this paper, a new approach used in the holographic lateral shear interferometry is considered, which is based on the shear of the object during the recording of holographic lateral shear interferograms and their optical processing. It is shown that, depending on the method of optical processing of these interferograms, several aberration-free interference patterns are observed simultaneously, reflecting with different sensitivities the changes in the light-wave phase introduced by the object. Due to the lateral shear, equal to or exceeding the linear size of the object, the interference patterns of the phase object are identical to interference patterns obtained in a two-beam, reference-wave interferometer.

2. Recording of holographic interferograms

To describe the observed interference patterns completely, we assume that the size of the object along the lateral shear direction during the recording of holographic interferograms does not exceed 1/4 of diameter of a probe light beam.

Let us select the coordinate system xyz in the following way. The x and y axes are oriented so that the x axis is directed along the shear of wave fronts in the recording plane of the interferogram, and the z axis is directed along the probe beam. The origin of the coordinate system xy is made coincident with the contour (circle) of the probe beam, as shown in Fig. 1a. Let us divide conditionally the region of the probe light beam and the adjacent region into five vertical zones of width s, which is equal to the lateral shear

A.M. Lyalikov Yanka Kupala Grodno State University, ul. Ozheshko 22, 230023 Grodno, Belarus; e-mail: amlialikov@grsu.by

Received 13 December 2006; revision received 11 April 2007
Kvantovaya Elektronika **38** (1) 64 – 68 (2008)
Translated by M.N. Sapozhnikov

of wave fronts produced in the lateral shear interferometer. Let us number the zones by 1, 2, 3, 4, and 5 (Fig. 1).

Let us assume that the linear dimensions of the phase object under study (triangle in Fig. 1) along the x axis are equal to the zone width s or smaller. This restriction does not concern the size of the object along the y axis. Consider the phase object located in zone 4, as shown in Fig. 1a. In this case, the phase distribution $\Phi_1(x, y)$ of the probe light beam with a plane wave front propagated through the phase object can be written in the convenient form

$$\Phi_1(x,y) = \begin{cases} \varepsilon(x,y) & \text{for zones } 2,\ 3,\ 5, \\ \varphi(x,y) + \varepsilon(x,y) & \text{for zone } 4, \end{cases} \tag{1}$$

where $\varepsilon(x, y)$ and $\varphi(x, y)$ are phase distortions characterising the deformation of the plane wave front caused by aberrations and its propagation through the phase object, respectively. The holographic lateral shear interferogram is recorded by superimposing two light beams obtained by dividing the probe-beam amplitude in the lateral shear interferometer (Fig. 1b). One of the beams propagates along the z axis and its phase is described by expression (1). Another beam is shifted along the x axis by the value s (for example, oppositely to the x axis direction) and is inclined to the first beam at some angle. Let us assume that the second light beam propagates in the plane yz. In this case, the phase distribution $\Phi_2(x, y)$ of the second light beam can be written in the form

$$\Phi_2(x,y) = \begin{cases} 2\pi\eta y + \varepsilon(x+s,y) & \text{for zones } 1,\ 2,\ 4, \\ 2\pi\eta y + \varphi(x+s,y) + \varepsilon(x+s,y) & \text{for zone } 3, \end{cases} \tag{2}$$

where $\eta = \cos\beta/\lambda$; β is the angle between the beam propagation direction and y axis; and λ is the wavelength.

Let us assume that the real amplitudes of interfering light beams are equal. In this case, we obtain from (1) and (2) the amplitude transmission of the first holographic lateral shear interferogram recorded before the displacement of the phase object under study:

$$\tau_1(x,y) \sim \tag{3}$$

$$\begin{cases} \{1+\cos[2\pi\eta y + \varepsilon(x+s,y) - \varepsilon(x,y)]\}^{-\gamma/2} & \text{for zone } 2, \\ \{1+\cos[2\pi\eta y + \varphi(x+s,y) + \varepsilon(x+s,y) - \varepsilon(x,y)]\}^{-\gamma/2} & \text{for zone } 3, \\ \{1+\cos[2\pi\eta y - \varphi(x,y) + \varepsilon(x+s,y) - \varepsilon(x,y)]\}^{-\gamma/2} & \text{for zone } 4, \end{cases}$$

where γ is the contrast coefficient of a photoemulsion [12].

Information on the phase object is present in zones 3 and 4, the bendings of holographic fringes caused by the object, described by functions $\varphi(x, y)$ and $\varphi(x + s, y)$, having opposite signs. In addition, according to (3), the holographic interferogram also contains residual aberrations, determined by the difference $[\varepsilon(x + s, y) - \varepsilon(x, y)]$.

Before recording the second holographic interferogram, the phase object is displaced from zone 4 (Fig. 1a) to zone 3 by the lateral shear value. The required accuracy of the shear can be provided in the following way. Before the displacement of the object, after the development of the photoemulsion, the first holographic interferogram is set to the recording position, which is controlled visually by making the object coincident with its image. A more accurate coincidence is achieved by obtaining an infinitely broad fringe in the moire pattern. Then, the object is

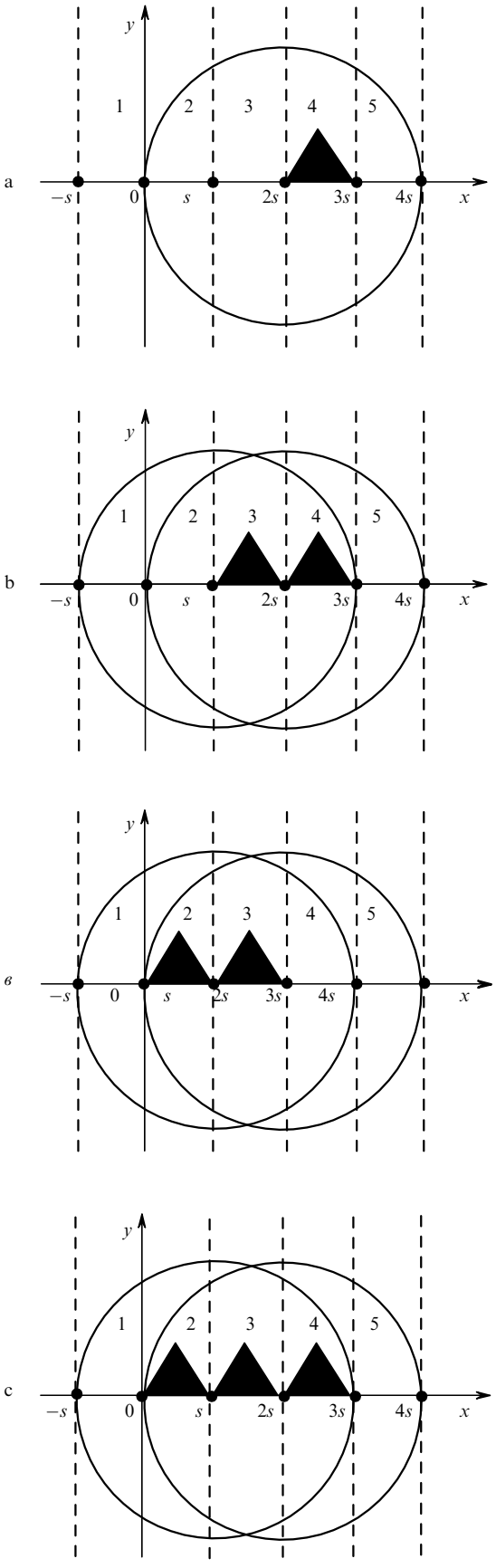

Figure 1. Geometrical images of light beam (circles) and object (triangles) contours in different planes upon recording and optical processing of holographic lateral shear interferograms; (1 – 5) zones of width s.

displaced from zone 4 (Fig. 1a) to zone 3 until its contour coincides with the left image of the object recorded in the holographic interferogram (Fig. 1b). The first holographic interferogram is removed from the interferometer and a new interferogram is recorded by superimposing waves with the phase distributions

$$\Phi_1'(x,y) = \begin{cases} \varepsilon(x,y) \text{ for zones 2, 4, 5,} \\ \varphi(x+s,y) + \varepsilon(x,y) \text{ for zone 3,} \end{cases} \tag{4}$$

$$\Phi_2'(x,y) = \begin{cases} 2\pi\eta y + \varepsilon(x+s,y) \text{ for zones 1, 3, 4,} \\ 2\pi\eta y + \varphi(x+2s,y) + \varepsilon(x+s,y) \text{ for zone 2.} \end{cases} \tag{5}$$

The amplitude transmission of the second holographic interferogram recorded after the displacement of the phase object is

$$\tau_2(x,y) \sim \tag{6}$$

$$\begin{cases} \{1+\cos[2\pi\eta y + \varphi(x+2s,y) + \varepsilon(x+s,y) - \varepsilon(x,y)]\}^{-\gamma/2} \text{ for zone 2,} \\ \{1+\cos[2\pi\eta y - \varphi(x+s,y) + \varepsilon(x+s,y) - \varepsilon(x,y)]\}^{-\gamma/2} \text{ for zone 3,} \\ \{1+\cos[2\pi\eta y + \varepsilon(x+s,y) - \varepsilon(x,y)]\}^{-\gamma/2} \text{ for zone 4.} \end{cases}$$

The holographic lateral shear interferogram (Fig. 1c), as in the previous case, is recorded in zones 2, 3, and 4, but information on the phase object under study is contained only in zones 2 and 3.

Consider several methods of optical processing of a pair of holographic interferograms of types (3) and (6), which differ in the realisation complexity and the sensitivity of detection of changes in the wave front introduced by the phase object.

3. Combined holographic interferograms

Figure 2 presents the known scheme of device for optical processing of a pair of combined holographic interferograms [12]. Holographic lateral shear interferograms described by expressions (3) and (6) are combined so that the left image of the phase object in the first (Fig. 1b) holographic interferogram coincided with the right image in the second (Fig. 1c) interferogram. Figure 1d presents the resulting image of the object in combined holographic interferograms. Combined holographic interferograms (*1*) (Fig. 2) are illuminated by a collimated light beam. Aperture (*3*) located in the image focal plane of objective (*2*) select the waves diffracted from the first and second holographic interferograms to the first diffraction order of the same sign. In this case, three interference images of the object will be observed in plane (*4*) optically conjugate with the plane of combined holographic interferograms (*1*) (Fig. 1d).

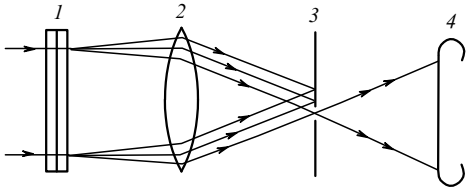

Figure 2. Scheme of a device for optical processing of a pair of combined holographic interferograms: (*1*) combined interferograms; (*2*) objective; (*3*) aperture; (*4*) plane optically conjugate with a plane of combined holographic interferograms (*1*).

The first image of the object is formed in zone 2 (Fig. 1d) due to interference, according to (3) and (6), of the waves

$$\begin{aligned} A_{1,2}(x,y) &= a_1 \exp\{\mathrm{i}[2\pi\eta y + \varepsilon(x+s,y) - \varepsilon(x,y)]\}, \\ A'_{1,2}(x,y) &= a_1 \exp\{\mathrm{i}[2\pi\eta y + \varphi(x+2s,y) \\ &\quad + \varepsilon(x+s,y) - \varepsilon(x,y)]\}, \end{aligned} \tag{7}$$

where a_1 is the real amplitude. The intensity distribution in the interference pattern of the object image located in zone 2 (Fig. 1d) is

$$I_2(x,y) \sim 1 + \cos[\varphi(x+2s,y)]. \tag{8}$$

One can see from expression (8) that aberrations $[\varepsilon(x+s,y) - \varepsilon(x,y)]$ in the interference pattern are excluded.

The second image is formed in zone 3 (Fig. 1d) due interference of the waves

$$\begin{aligned} A_{1,3}(x,y) &= a_1 \exp\{\mathrm{i}[2\pi\eta y + \varphi(x+s,y) \\ &\quad + \varepsilon(x+s,y) - \varepsilon(x,y)]\}, \\ A'_{1,3}(x,y) &= a_1 \exp\{\mathrm{i}[2\pi\eta y - \varphi(x+s,y) \\ &\quad + \varepsilon(x+s,y) - \varepsilon(x,y)]\}. \end{aligned} \tag{9}$$

The intensity distribution in the interference pattern of the object image located in zone 3 (Fig. 1d) has the form

$$I_3(x,y) \sim 1 + \cos[-2\varphi(x+s,y)]. \tag{10}$$

Aberrations in this interference pattern, as in the interference pattern observed in zone 2, are completely excluded. It follows from expression (10) that the interference pattern in zone 3 (Fig. 1d) reflects with the doubled sensitivity the changes in the phase caused by the object displaced along the x axis by the value $-s$ with respect to its initial position (Fig. 1a) corresponding to the recording of the first holographic interferogram. Note that the signs in front of functions describing phase variations caused by the object in zones 2 and 3 are opposite. This will lead to mutually opposite bending of interference fringes of finite width in these zones. The measurement sensitivity for the interference pattern in zone 3 is doubled due to the overlap of displaced images of the object, reconstructed from the first and second holographic interferograms.

The last image is formed in zone 4 (Fig. 1d) due to interference of the waves

$$\begin{aligned} A_{1,4}(x,y) &= a_1 \exp\{\mathrm{i}[2\pi\eta y - \varphi(x,y) \\ &\quad + \varepsilon(x+s,y) - \varepsilon(x,y)]\}, \\ A'_{1,4}(x,y) &= a_1 \exp\{\mathrm{i}[2\pi\eta y + \varepsilon(x+s,y) - \varepsilon(x,y)]\}. \end{aligned} \tag{11}$$

The intensity distribution in the interference pattern of the object image located in zone 4 (Fig. 1d) is similar to that in zone 2:

$$I_4(x,y) \sim 1 + \cos[\varphi(x,y)]. \tag{12}$$

When holographic interferograms described by expressions (3) and (6) are made exactly coincident, the infinite-width fringe pattern is observed.

Expressions (8), (10), and (12) describe infinite-width fringe patterns. Finite-width fringe patterns can be obtained by two methods, which are considered in detail in [12]. Finite-width fringe patterns can be obtained in this method of optical processing of holographic interferograms by slightly turning, for example, one of the interferograms.

Photographs in Fig. 3 show the infinite- and finite-width fringe patterns of the object obtained by the above-described method of optical processing of a pair of combined holographic interferograms. These fringe patterns reflect changes in the wave front of the object wave propagated through the object under study – a cylindrical laser crystal of diameter 3.5 mm and length 51 mm with polished plane–parallel end-faces. The lateral shear and corresponding displacement of the crystal were 3.5 mm.

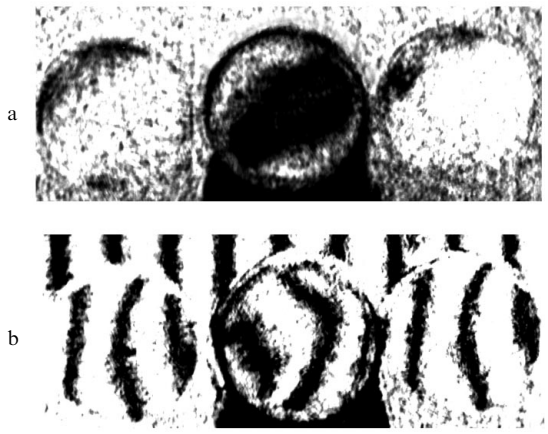

Figure 3. Infinite- (a) and finite-width (b) fringe patterns of the object under study obtained after optical processing of a pair of combined holographic interferograms.

Finite-width fringe patterns were obtained by rotating one of the holographic interferograms through a small angle. Note, however, that in this case the displacement of the object image was observed with respect to the image fixed in the holographic interferogram. This displacement increased with decreasing the period of interference fringes, which was undesirable.

4. Optically conjugate holographic interferograms

The method of optical processing of a pair of holographic interferograms considered below is more complicated, but offers a number of advantages.

Figure 4 presents the scheme of a device for optical processing of a pair of optically conjugate holographic interferograms. Such a scheme was used earlier for optical processing of the object and reference holograms of phase objects [12] and a pair of holographic lateral shear interferograms displaced with respect to each other [11]. The main advantage of the scheme is the possibility of obtaining fringe patterns providing considerably higher measurement sensitivity. Therefore, we will consider this method of optical processing of holographic interferograms only for the interference image corresponding to the maximum sensitivity of detecting wave-front changes caused by the object under study (interference image of zone 3 in Fig. 1d).

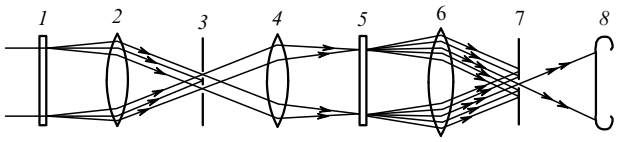

Figure 4. Scheme of a device for optical processing of a pair of optically conjugate holographic interferograms: (*1*, *5*) holographic interferograms; (*2*, *4*, *6*) objectives; (*3*, *7*) apertures; (*8*) plane optically conjugate with planes of holographic interferograms (*1*) and (*5*).

Holographic interferograms (*1*) and (*5*) (Fig. 4) are mounted in planes optically conjugate to objectives (*2*) and (*4*). Upon illumination of the first holographic interferogram, for example, of type (3), the waves

$$\begin{aligned} A_{n,3}(x,y) &= a_n \exp\{\mathrm{i}[2\pi n\eta y + n\varphi(x+s,y) \\ &\quad + n\varepsilon(x+s,y) - n\varepsilon(x,y)]\}, \\ A^*_{n,3}(x,y) &= a_n \exp\{-\mathrm{i}[2\pi n\eta y + n\varphi(x+s,y) \\ &\quad + n\varepsilon(x+s,y) - n\varepsilon(x,y)]\} \end{aligned} \tag{13}$$

diffract in complex conjugate nth orders ($n = 1, 2, 3\ldots$) in zone 3 (Fig. 1d), where a_n is the real wave amplitude. Waves of type (13) in the image plane of objective (*2*) are separated from other diffraction orders by two holes in aperture (*3*). The selected waves are collimated with objective (*4*) and illuminate the second holographic interferogram (*5*) of type (6). The distribution of complex amplitudes at the output of the second holographic interferogram is described by the expression $|A_{n,3}(x,y)+A^*_{n,3}(x,y)|\tau_2(x,y)$. Taking (6) and (13) into account, we can show that the waves

$$\begin{aligned} B_{n,3}(x,y) &= b_n \exp[\mathrm{i}2n\varphi(x+s,y)], \\ B^*_{n,3}(x,y) &= b_n \exp[-\mathrm{i}2n\varphi(x+s,y)], \end{aligned} \tag{14}$$

diffracted to the nth orders will propagate normally to the second holographic interferogram (*5*), where b_n is the real wave amplitude. Waves of type (14) are selected in the image focal plane of objective (*6*) by aperture (*7*) and form the interference pattern

$$I_{n,3}(x,y) \sim 1 + \cos[-4n\varphi(x+s,y)] \tag{15}$$

in plane (*8*) optically conjugate with holographic interferograms (*1*) and (*5*).

This interference pattern reflects with the $4n$-fold enhancement of the sensitivity the changes in the wave front of the object wave caused by the object under study.

Figure 5 presents the interference images of zone 3 (Fig. 1d) obtained after optical processing of a pair of holographic interferograms located in optically conjugate planes by selecting the ±2th (Fig. 5a) and ±3th (Fig. 5b) diffraction orders. According to expression (15), the sensitivity of measuring these interference patterns is 8 and 12 times higher, respectively, than that for the interference patterns of the crystal under study observed in zones 2 and 4 (Fig. 3) by using the previous method of optical processing.

Figure 5. Interference patterns obtained after optical processing of a pair of holographic interferograms located in optically conjugate planes; the measurement sensitivity is higher by 8 (a) and 12 (b) times.

5. Conclusions

Thus, the methods of optical processing of holographic lateral shear interferograms recorded by displacing the object under study allow one to obtain simultaneously several, in particular, three aberration-free interference patterns, which reflect with different sensitivities the changes in the light-wave phase caused by the object under study. The methods differ in the complexity of their realisation and the maximum measurement sensitivity.

Note that, if for the first and second methods of optical processing only the central mage of the interference pattern should be obtained with the enhanced sensitivity, then the linear size and, hence, the shear value with respect to the probe beam diameter can be increased. In this case, the length of the object along the later shear direction should not exceed half the diameter of the probe beam, and the lateral shear should be equal to half the beam diameter.

Acknowledgements. The author thank A.V. Sutyagin for his help in processing lateral shear holograms and obtaining interference patterns.

References

1. Waetzmann E. *Annalen der Physik*, **39**, 1042 (1912).
2. Malacara D. (Ed.) *Optical Shop Testing* (New York: John Wiley & Sons, 1992).
3. Shekhtman V.N., Rodinov A.Yu., Pel'menev A.G. *Opt. Spektrosk.*, **76**, 988 (1994).
4. Bashkin A.S., Korotkov P.I., Maksimov Yu.P., et al. *Kvantovaya Elektron.*, **24**, 786 (1997) [*Quantum Electron.*, **27**, 766 (1997)].
5. Toker G.R., Levin D. *Appl. Opt.*, **37**, 5162 (1998).
6. Santhanakrishnan T., Palanisamy P.K., Sirohi R.S. *Appl. Opt.*, **37**, 3447 (1998).
7. Ivanov P.V., Koryabin A.V., Shmal'gauzen V.I. *Kvantovaya Elektron.*, **27**, 78 (1999) [*Quantum Electron.*, **29**, 360 (1999)].
8. Sokolov V.I. *Kvantovaya Elektron.*, **31**, 891 (2001) [*Quantum Electron.*, **31**, 891 (2001)].
9. Komissaruk V.A., in *Issledovaniya prostranstvennykh gazodinamicheskikh techenii na osnove opticheskikh metodov. Trudy VVIA im. N.E. Zhukovskogo* (Optical Studies of Spatial Gas-Dynamic Flows, Proceedings of N.E. Zhukovskii VVIA) (Moscow, 1971).
10. Lyalikov A.M. *Kvantovaya Elektron.*, **35**, 290 (2005) [*Quantum Electron.*, **35**, 290 (2005)].
11. Lyalikov A.M. *Opt. Spektrosk.*, **99**, 151 (2005).
12. Beketova A.K., Belozerov A.F., Berezkin A.N., et al. *Golografichskaya interferometriya fazovykh ob'ektov* (Holographic Interferometry of Phase Objects) (Leningrad: Nauka, 1979).